

Energy & Environmental Science

Accepted Manuscript



This is an *Accepted Manuscript*, which has been through the Royal Society of Chemistry peer review process and has been accepted for publication.

Accepted Manuscripts are published online shortly after acceptance, before technical editing, formatting and proof reading. Using this free service, authors can make their results available to the community, in citable form, before we publish the edited article. We will replace this *Accepted Manuscript* with the edited and formatted *Advance Article* as soon as it is available.

You can find more information about *Accepted Manuscripts* in the [Information for Authors](#).

Please note that technical editing may introduce minor changes to the text and/or graphics, which may alter content. The journal's standard [Terms & Conditions](#) and the [Ethical guidelines](#) still apply. In no event shall the Royal Society of Chemistry be held responsible for any errors or omissions in this *Accepted Manuscript* or any consequences arising from the use of any information it contains.

Sr_{3-3x}Na_{3x}Si₃O_{9-1.5x} (x=0.45) as a Superior Solid Oxide-ion Electrolyte for Intermediate-temperature Solid Oxide Fuel Cells

Tao Wei¹, Preetam Singh², Yunhui Gong¹, John B. Goodenough², Yunhui Huang³ and Kevin Huang^{1*}

¹ Department of Mechanical Engineering, University of South Carolina, Columbia, SC29201, USA

² Texas Materials Institute, The University of Texas at Austin, Austin, TX78713, USA

³ School of Materials Science and Engineering, Huazhong University of Science and Technology, Wuhan, Hubei 430074, China

*E-mail: kevin.huang@sc.edu

ABSTRACT

We here report that a newly discovered superior oxide-ion conductor Sr_{3-3x}Na_{3x}Si₃O_{9-1.5x} (x=0.45) (SNS) demonstrates full potential to be a practical solid electrolyte for intermediate-temperature solid oxide fuel cells (IT-SOFCs). It exhibits the highest oxide-ion conductivity with the lowest activation energy among all the chemically stable solid oxide-ion conductors reported. The ionic conductivity is stable over a broad range of partial pressure of oxygen (10⁻³⁰~1 atm) for an extended period of time. A SOFC based on a 294-μm thick SNS-electrolyte produces peak power densities of 431 and 213 mW·cm⁻² at 600 and 500°C, respectively. Considering its competitive costs in materials and manufacturing and rare-earth free composition, SNS has great potential to become a new class of technologically and strategically important electrolytes for commercial IT-SOFCs.

Keywords: solid oxide-ion electrolyte; ionic conductivity; electrode polarization; power density; solid oxide fuel cell

INTRODUCTION

For the past half a century, the clean and efficient solid oxide fuel cell (SOFC) technology has been developed to the stage that a further reduction in operating temperature from the current $\geq 800^\circ\text{C}$ to $\leq 600^\circ\text{C}$ is necessary in order for it to commercially compete with internal combustion engines.^{1,2} Fast oxide-ion conductors are a key functional component determining the operating temperature of a solid oxide fuel cell. With the existing oxide-ion conductor systems such as Y_2O_3 -stabilized ZrO_2 , Gd_2O_3 -doped CeO_2 and Sr- and Mg-doped LaGaO_3 , it would seem to be very difficult to achieve such reduced-temperature SOFCs at commercial scale.

It is very interesting to note that all the existing oxide-ion conductors possess one of the following crystal structures: fluorite, perovskite and apatite.³⁻¹¹ Recently, a new family of superior solid oxide-ion conductors with a 2D layered structure and generic formula of $\text{Sr}_{3-3x}\text{A}_{3x}\text{Si}_{3-3y}\text{Ge}_{3y}\text{O}_{9-1.5(x+y)}$ (A=Na, K) has been identified as a promising electrolyte for intermediate-temperature solid oxide fuel cells (IT-SOFCs).^{12,13} Since Si^{4+} has a strong tetrahedral site preference, $\text{Sr}_3\text{Si}_3\text{O}_9$ does not crystallize in the perovskite structure. Instead, it forms a layered $(\text{SrSiO}_3)_3$ structure containing close-packed planes of Sr^{2+} in trigonal-prismatic coordination separated by a layer of Si_3O_9 units containing three SiO_4 tetrahedra sharing corners in a triangular plane of oxygen parallel to the Sr^{2+} planes.¹² The apical oxide ions of the tetrahedra coordinate the Sr^{2+} and have a close approach to oxygen sites on neighboring Si_3O_9 complexes. Substitution of K^+ or Na^+ for Sr^{2+} introduces mobile oxygen vacancies,^{12,13} and steric constraints prevent the vacancies from being eliminated by corner

sharing Si_3O_9 unit. $\text{Sr}_{3-3x}\text{K}_{3x}\text{Si}_3\text{O}_{9-1.5x}$ is hygroscopic while $\text{Sr}_{3-3x}\text{Na}_{3x}\text{Si}_3\text{O}_{9-1.5x}$ is not. A neutron-diffraction study at different temperatures has suggested that oxygen vacancies are retained by the steric hindrance with substitution of either K^+ or Na^+ for Sr^{2+} ; ¹⁴ the vacancies occupy primarily M_3O_9 ($\text{M} = \text{Si}, \text{Ge}$) complexes at lower temperatures with increasing apical-site occupancy as the temperature is raised. An ongoing research in authors' groups is focused on understanding the dynamics of fast oxygen transport in the new electrolyte material using *in-situ* solid-state NMR technique.

The best oxide-ion conductivity of the $\text{Sr}_{3-3x}\text{A}_{3x}\text{Si}_{3-3y}\text{Ge}_{3y}\text{O}_{9-1.5(x+y)}$ ($\text{A}=\text{Na}, \text{K}$) series is found in the composition $\text{Sr}_{3-3x}\text{Na}_{3x}\text{Si}_3\text{O}_{9-1.5x}$ ($x=0.45$) (herein referred to as SNS). At 500°C , the measured oxide-ion conductivity is $>10^{-2}$ S/cm, which is equivalent to that of $\text{La}_{0.80}\text{Sr}_{0.20}\text{Ga}_{0.83}\text{Mg}_{0.17}\text{O}_{3-\delta}$ (LSGM) at 600°C ¹⁵⁻¹⁷ and of $\text{Zr}_{0.92}\text{Y}_{0.08}\text{O}_{2-\delta}$ (YSZ) at 670°C . ¹⁸ It has also been reported that SNS is chemically stable in reducing atmospheres and compatible with commonly used SOFC cathodes. ^{12, 13} Therefore, use of SNS as a functional electrolyte in a SOFC is expected to appreciably reduce the operating temperature of the latter and finds its utility in commercial IT-SOFCs. However, until now, this promise has not yet been fully demonstrated in SOFCs. In this study, we report for the first time the characteristics of SNS as a truly functional electrolyte in a SOFC and electrochemical performance of a SNS-based SOFC operated at $500\text{-}600^\circ\text{C}$.

EXPERIMENTAL SECTION

Synthesis and characterization of the SNS electrolyte

The SNS samples were synthesized through a two-step solid-state reaction route. The starting materials of SrCO_3 (Aldrich, 99.9%), SiO_2 (Alfa Aesar, 99.5%), and Na_2CO_3 (Fisher Scientific, 99.9%) were first intimately mixed in a stoichiometric ratio, followed by pelletizing under a static pressure of 200 MPa and calcining at 1000°C for 20 hours. After breaking up and ball milling to submicron powders, the SNS powder was pelletized again and finally sintered at 1050°C for another 20 hours to densification. To avoid reactions between SNS and Al_2O_3 boat, a layer of loose $\text{Sr}_{3-3x}\text{Na}_{3x}\text{Si}_3\text{O}_{9-1.5x}$ ($x=0.45$) powders was spread over the surface of Al_2O_3 prior to sintering.

The oxide-ion conductivity of the dense SNS pellets (~ 0.5 cm in thickness and ~ 1.5 cm in diameter) was measured in the temperature range of 450 - 700°C by a Solartron Electrochemical 1260/1287 system using Electrochemical Impedance Spectroscopy (EIS) technique. The frequency was swept from 0.5 to 10^6 Hz with an AC stimulus of 10 mV to generate impedance spectra fully covering the grain and grain-boundary responses. Silver paste/mesh was used as the current collector for the measurement.

The phase purity of SNS after sintering and exposure to reducing atmospheres was examined by powder X-ray diffraction (PXRD) using an X-ray diffractometer (D/max-A, Rigaku, Japan) with graphite-monochromatized $\text{CuK}\alpha$ radiation ($\lambda=1.5418$ Å). The XRD scan was performed at a rate of 5°min^{-1} from $2\theta=20$ to 80° . The XRD patterns were further analyzed with the JADE (MDI) software to identify phase structure and compositions.

The thermal expansion of the SNS was measured in a flowing air from RT to 1000°C with a Theta 1600 dilatometer. The coefficient of thermal expansion (TEC) as a function of

temperature was determined as the derivative of a change in length with regard to temperature.

Electrochemical evaluation of the SNS-based cells

Two types of cells, *viz.* half-cell *vs* full-cell, were fabricated based on a symmetrical ceramic structure of porous-SNS/dense-SNS/porous-SNS. The symmetrical half-cell configuration was intended to study the cathode polarization only, whereas the full-cell counterpart was aimed to evaluate the true electrochemical performance of a SNS-based SOFC. There were two steps involved in making each type of cell. The first step was to fabricate the two symmetrical porous SNS scaffolds on two sides of a dense SNS membrane. To do so, a ~30- μm thick organic-loaded SNS layer was first screen printed on each side of the dense SNS membrane, followed by firing it at 1000°C for 1 hour to obtain porosity in the thin SNS-coating and achieve a good bonding with the dense SNS membrane. The second step was to infiltrate the respective electrode nanoparticles into the prefabricated symmetrical porous SNS scaffolds through nitrate solutions. After each infiltration, the cell was fired at 400°C for 1 hour to decompose nitrates into oxides. After a total of seven infiltration-decomposition steps, the infiltrated cell was finally fired at 800°C for 1 hour to form the wanted phase. For the symmetrical half-cell cathode polarization study, a nitrate solution containing stoichiometric amount of Sm, Sr and Co were impregnated equally into the two porous SNS scaffolds to yield two identical $\text{Sm}_{0.5}\text{Sr}_{0.5}\text{CoO}_{3-\delta}$ (SSC)/SNS composite cathode. For the fuel-cell performance evaluation, one side of the porous SNS scaffold was infiltrated with SSC to serve as the cathode and another side with Ni nanoparticles to serve as the anode.

The effective surface area of cells was kept at 0.5 cm². Silver past/mesh was used as the current collector for all the electrochemical evaluations.

The electrochemical performance of thus fabricated cells was characterized by the same Solartron 1260/1287 system used for oxide-ion conductivity with similar sweeping frequency range and stimulus AC signal. The DC functionality of the system was utilized to attain the characteristic V-I and P-I curves. The testing temperature was focused on intermediate temperature ranging from 500 to 600°C. A flow of 50 ml·min⁻¹ air and 30 ml·min⁻¹ dry H₂ was employed as as the oxidant and fuel, respectively. A commercial glass (Schott AG, Standort Landshut, GM 31107) was used to seal the testing SOFC.

Microstructural evaluation of the SNS-based cells

The microstructural features of and compositional distributions across both the half-cells and single fuel-cells studied were captured and analyzed with a field emission scanning electron microscope (FESEM, Zeiss Ultra) equipped with an energy dispersive X-ray spectroscopy (EDS) analyzer, respectively.

RESULTS AND DISCUSSION

Oxide-ion conductivity

The measured oxide-ion conductivity of the SNS is compared in the temperature range of 450-700°C in Fig.1 with other well-known chemically stable oxide-ion conductors having crystal structures of fluorite, perovskite and apatite. The Bi₂O₃-based oxide-ion conductors

are not included in the comparison for the fact that they are not chemically stable in reducing atmospheres. The exceptionally low activation energy E_a is a unique feature of the SNS, making it ideal for use as an electrolyte in reduced temperature (<600°C) SOFCs. It is believed that the easy migration of oxide-ion vacancies with a zigzag pathway in the basal plane is the origin of low activation energy observed.^{12,13} We are currently using in-situ solid state NMR to reveal more details on the dynamics of oxide-ion transport in SNS. Due to the fact that our data were focused within a narrower temperature range than ref. [13], the defects-association related curvature behavior is not so evident in Fig.1.

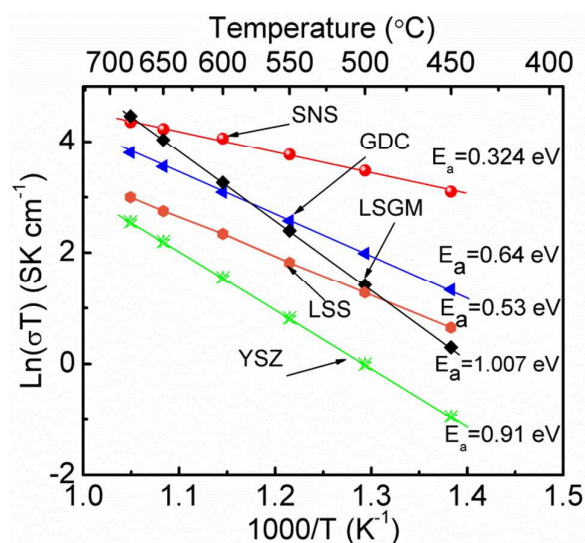


Fig.1 Comparison of oxide-ion conductivity of SNS measured in air with other well-known oxide-ion conductors. LSGM – ref [17]; YSZ – ref [18]; GDC – ref [19]; Sr doped $\text{La}_{10}\text{Si}_6\text{O}_{27}$ (LSS) apatite – ref [20]

The independence of conductivity on partial pressure of oxygen ($p\text{O}_2$) is a key indicator of pure oxide-ion conductors and electronic insulators. Fig.2 shows the ionic conductivity measured over a $p\text{O}_2$ ranging from oxidizing pure O_2 to reducing 5% H_2 - N_2 in a temperature range of 500-650°C. No apparent $p\text{O}_2$ -dependence of conductivity is observed over a $p\text{O}_2$

window as wide as $10^{-30} \sim 1$ atm, suggesting that SNS is indeed a pure and chemically stable oxide-ion conductor.

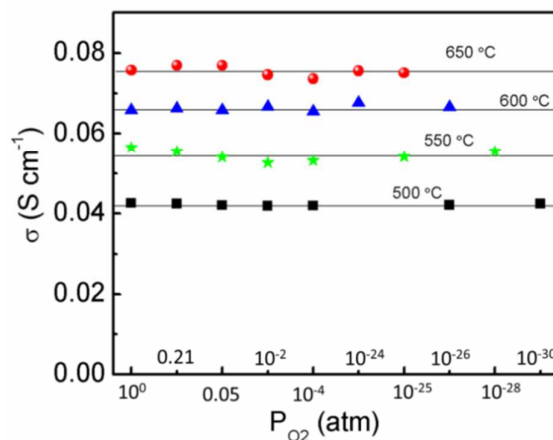


Fig.2 Variation of oxide-ion conductivity of SNS with pO_2 at 500-650°C

The stability of oxide-ion conductivity over time is another important characteristic for a practically meaningful oxide-ion conductor. Fig.3 shows the oxide-ion conductivity of SNS measured in two extreme atmospheres: air and 5% H_2 - N_2 , at 600°C, over a 200-hour period. No obvious change in conductivity is observed, suggesting that the oxide-ion conducting phase in the SNS is stable. This observation is consistent with Fig.4, where XRD patterns of the sample are shown unchanged after the exposure to dry 5% H_2 - N_2 even pure H_2 .

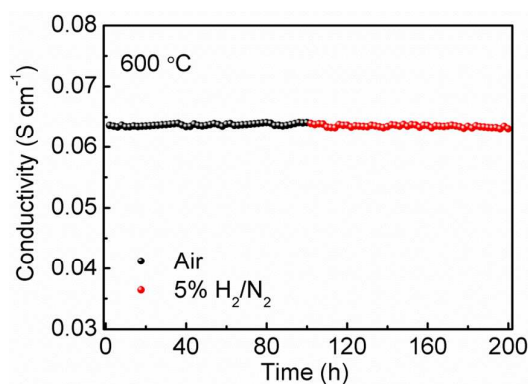


Fig.3 Oxide-ion conductivity of SNS as a function of time measured in air and dry 5% H_2 - N_2

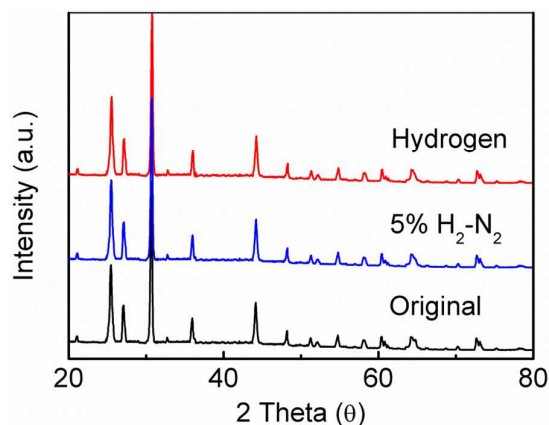


Fig.4 Comparison of XRD patterns of SNS before and after exposure to 5%H₂-N₂ and pure hydrogen

Microstructure

The dense microstructure of SNS after densification at 1050°C is shown in Fig.5 from surface as well as fracture. Compared to other commonly known oxide-ion conductor counterparts, low-temperature densification (1050°C) for the SNS implies lower manufacturing cost. This feature combined with the fact that SNS uses inexpensive and rare-earth-free constituents makes the new electrolyte an ideal, cost-competitive and strategically important solid electrolyte for commercial IT-SOFCs.

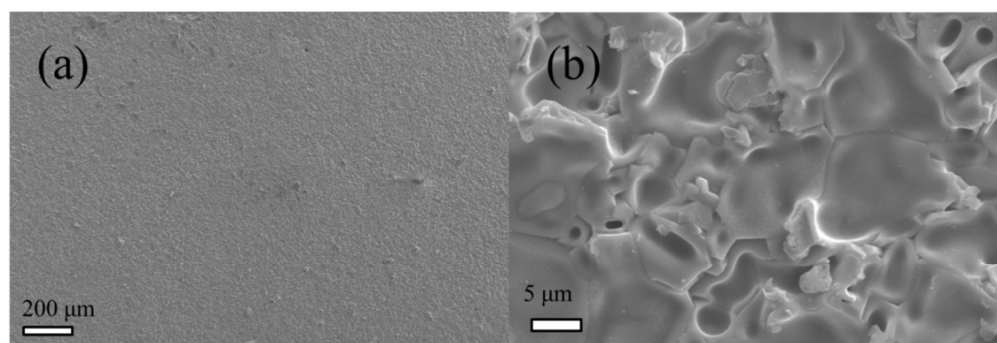


Fig.5 SEM images of a dense SNS electrolyte; (a) surface morphology; (b) cross-section

Thermal expansion coefficient (TEC)

A good thermal expansion match between any two adjacent components in a SOFC endures the latter to repeated thermal transients. Fig.6 shows the variation of TEC with temperature from RT to 1000°C. The obtained average TEC= $12.1 \times 10^{-6} \text{ K}^{-1}$ is deemed manageable with most active electrode materials. The TEC mismatch issue can also be mitigated if high-TEC electrodes are dispersed as nanoparticles and supported by a SNS skeleton as demonstrated in this study.

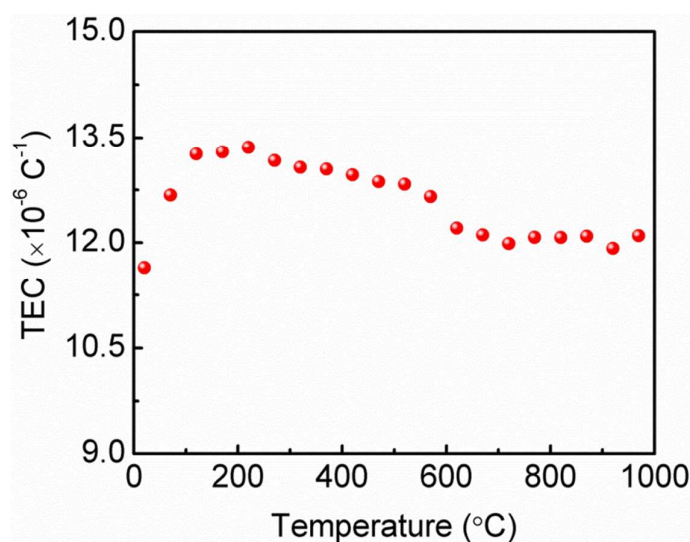


Fig.6 Thermal expansion coefficient of SNS measured from RT to 1000°C

With an excellent oxide-ion conductor identified, lowering electrode polarizations would be the next priority to achieve the ultimate high power density of a SOFC. As described in the Experimental Section, a co-sintered symmetrical structure consisting of a thick SNS membrane coated with two thin identical porous SNS scaffolds impregnated with active electrode nanoparticles was adopted as the electrodes for reducing electrode polarizations. The cross-sectional views of the three-layer microstructures are shown in Fig.7. From these

SEM images, it is evident that submicron SSC particles are well-connected and dispersed within the SNS skeleton, which ensures a good oxygen reduction reaction activity and electronic conductivity.

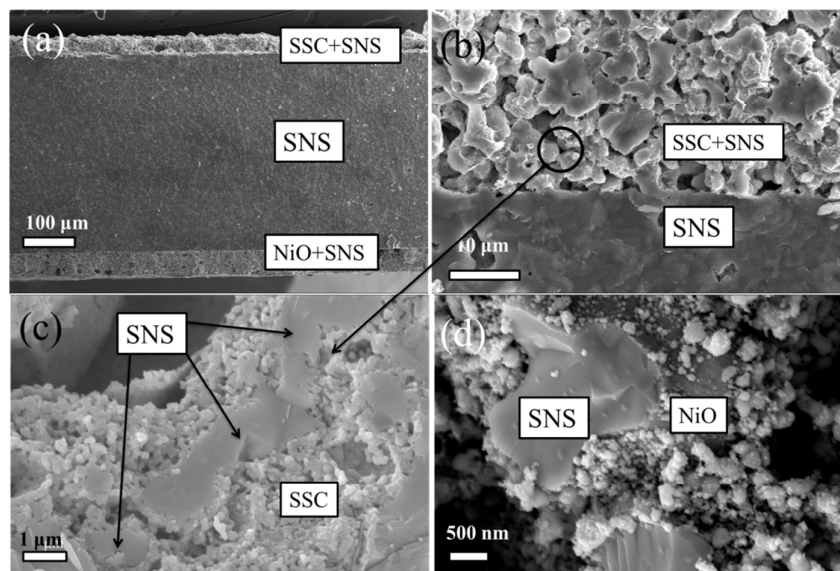


Fig.7 Microstructures of a SNS-supported SOFC; (a) overall view of the three functional layers; (b) cathode view; (c) magnified cathode view; (d) magnified anode view

The performance of a composite cathode SSC/SNS was first evaluated by EIS using the symmetrical cell configuration as described in the Experimental Section. Fig.8 shows the spectra measured at 600°C in air. To show the advantage of SNS over LSGM, a similarly structured LSGM symmetrical cell with the same thickness (~230μm for this case) and infiltrated cathode SSC was also made and tested. The comparison shown in Fig.8 indicates an ohmic resistance of 0.350 Ω·cm² for SNS, but as high as 0.664 Ω·cm² for LSGM, at 600°C. The difference in electrode polarization is even more revealing: 0.266 Ω·cm² for the SNS-cell and 0.784 Ω·cm² for the LSGM-cell. Higher oxide-ion conductivity of the SNS clearly plays a key role in reducing ohmic and electrode polarization resistances observed.

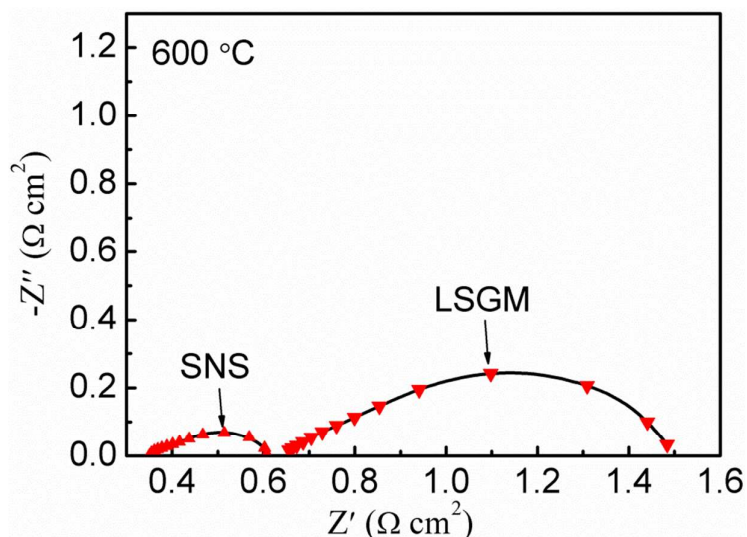


Fig.8 Comparison of EIS spectra of SSC-SNS/SNS/SSC-SNS and SSC-LSGM/LSGM/SSC-LSGM symmetrical cells measured in air.

The electrochemical performance of a 294- μm thick SNS-supported single SOFC with infiltrated electrode nanoparticles was evaluated from 500 to 600 $^{\circ}\text{C}$, the results of which are shown in Fig.9. The peak power density reached 431 $\text{mW}\cdot\text{cm}^{-2}$ at 600 $^{\circ}\text{C}$ and 213 $\text{mW}\cdot\text{cm}^{-2}$ at 500 $^{\circ}\text{C}$, respectively. The power densities observed at such intermediate temperatures for a SOFC with such a thick electrolyte membrane are very impressive. Compared to the best peak power density reported for a 200- μm LSGM-based SOFC, *viz.* 200 $\text{mW}\cdot\text{cm}^{-2}$ at 600 $^{\circ}\text{C}$,²¹ this performance represents a more than 2-fold power enhancement. As the temperature and the thickness of the electrolyte are further reduced, which is an ongoing research in the authors' lab, the degree of the enhancement would be even greater. The appreciable power enhancement is believed to be closely associated with the high ionic conductivity and low activation energy of the SNS electrolyte.

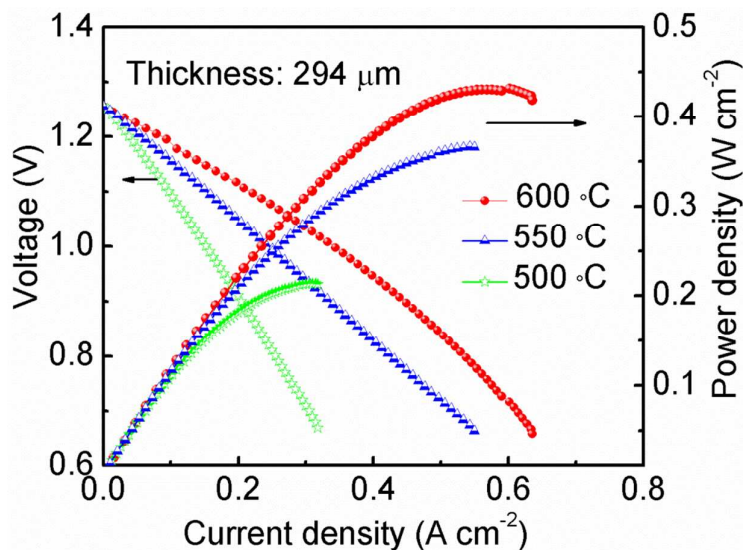


Fig.9 Electrochemical performance of a 294- μm thick SNS-supported SOFC with infiltrated electrode nanoparticles

CONCLUSIONS

In summary, the newly discovered 2D layered $\text{Sr}_{1-3x}\text{Na}_{3x}\text{Si}_3\text{O}_{9-1.5x}$ ($x=0.45$) (SNS) has been fully characterized as an electrolyte material for IT-SOFCs. Its oxide-ion conductivity is the highest with the lowest activation energy among all the chemically stable oxide-ion conductors reported. The purity of oxide-ion conduction has also been confirmed by the independence of ionic conductivity on $p\text{O}_2$. The stable ionic conductivity over time further illustrates its potential to be a practical electrolyte for commercial IT-SOFCs. The electrochemical performance of a 294- μm thick-film SNS-supported SOFC is very promising, reaching peak power densities of 431 and 213 $\text{mW}\cdot\text{cm}^{-2}$ at 600 and 500 $^\circ\text{C}$, respectively. Overall, it is concluded that SNS is a superior oxide-ion conductors well suited for IT-SOFCs. Considering its competitive costs in materials and manufacturing and rare-earth free

composition, SNS has great potential to become a new class of technologically and strategically important electrolytes for commercial IT-SOFCs.

Acknowledgements

KH would like to thank NSF (CBET-1340269, CBET-124706) and the U. S. Army Research Laboratory and the U. S. Army Research Office (W911NF-10-R-006) for financial support.

JBG thanks the Robert A. Welch Foundation of Houston, TX for financial support.

Notes and References

- 1 A. J. Jacobson, *Chem. Mater.*, 2009, **22**, 660-674.
- 2 A. Agüero, L. Fawcett, S. Taub, R. Woolley, K.-T. Wu, N. Xu, J. Kilner and S. Skinner, *J. Mater. Sci.*, 2012, **47**, 3925-3948.
- 3 A. Chroneos, B. Yildiz, A. Tarancon, D. Parfitt and J. A. Kilner, *Energy Environ. Sci.*, 2011, **4**, 2774-2789.
- 4 P. M. Panchmatia, A. Orera, E. Kendrick, J. V. Hanna, M. E. Smith, P. R. Slater and M. S. Islam, *J. Mater. Chem.*, 2010, **20**, 2766-2772.
- 5 S. Tao and J. T. S. Irvine, *Mater. Res. Bull.*, 2001, **36**, 1245-1258.
- 6 T. Liao, T. Sasaki, S. Suehara and Z. Sun, *J. Mater. Chem.*, 2011, **21**, 3234-3242.
- 7 L. Malavasi, C. A. J. Fisher and M. S. Islam, *Chem. Soc. Rev.*, 2010, **39**, 4370-4387.

- 8 S. Nakayama, T. Kageyama, H. Aono and Y. Sadaoka, *J. Mater. Chem.*, 1995, **5**, 1801-1805.
- 9 H. Yoshioka, T. Mitsui, A. Mineshige and T. Yazawa, *Solid State Ionics*, 2010, **181**, 1707-1712.
- 10 J. E. H. Sansom, J. R. Tolchard, M. S. Islam, D. Apperley and P. R. Slater, *J. Mater. Chem.*, 2006, **16**, 1410-1413.
- 11 D. Marrero-López, M. C. Martín-Sedeño, J. Peña-Martínez, J. C. Ruiz-Morales, P. Núñez, M. A. G. Aranda and J. R. Ramos-Barrado, *J. Power Sources*, 2010, **195**, 2496-2506.
- 12 P. Singh, and J. B. Goodenough, *J. Am. Chem. Soc.*, 2013, **135**, 10149-10154.
- 13 P. Singh, and J. B. Goodenough, *Energy Environ. Sci.*, 2012, **5**, 9626-9631.
- 14 P. Singh and J. B. Goodenough, manuscript in preparation.
- 15 T. Ishihara, H. Matsuda, and Y. Takita, *J. Am. Chem. Soc.*, 1994, **116**, 3801-3803.
- 16 M. Feng, and J. B. Goodenough, *Eur. J. Solid State Inorg. Chem.*, 1994, **T31**, 663-672.
- 17 K. Huang, R. Tichy, and J. B. Goodenough, *J. Am. Ceram. Soc.*, 1998, **81(10)**, 2565-2575.
- 18 D. W. Strickler, and W.G. Carlson, *J. Am. Ceram. Soc.*, 1965, **48**, 286-289.
- 19 B. C. H. Steele, *Solid State Ionics*. 2000, **129**, 95-110.
- 20 H. Arikawa, H. Nishiguchi, T. Ishihara and Y. Takita, *Solid State Ionics*, 2000, **136-137**, 31-37.
- 21 J.-H. Wan, J.-Q. Yan, and J. B. Goodenough, *J. Electrochem. Soc.*, 2005, **152**, A1511-A1515.